04,10

The influence of heat treatment on the memristive properties of Cu/$(Co_{40}Fe_{40}B_{20})_x(SiO_2)_{100-x}$/$LiNbO_3$/Cr/Cu/Cr capacitor structures

© A.V. Sitnikov[1,2], Yu.E. Kalinin[1], I.V. Babkina[1], A.E. Nikonov[1], A.R. Shakurov[1,¶], M.N. Kopytin[1]

[1] Voronezh State Technical University,
Voronezh, Russia
[2] National Research Center „Kurchatov Institute“,
Moscow, Russia

¶ E-mail: Aleks.shakurov@mail.ru

Received July 19, 2024
Revised August 10, 2024
Accepted August 11, 2024

The paper reveals the results of a study of the effect of heat treatment up to 500°C on the memristive properties of Cu/$(Co_{40}Fe_{40}B_{20})_{35.5}(SiO_2)_{64.5}$/$LiNbO_3$/Cr/Cu/Cr/glass-ceramic capacitor type structure. It has been shown that heat treatment up to 350°C for 60 min does not change the cyclic endurance of the samples ($> 10^4$), increases the ratio of the high-resistance resistive state (R_{off}) to the low-resistance resistive state (R_{on}) from 25 in the original state to 60 in the heat-treated state and reduces the values of resistive switching voltages to ± 4 V. Heat treatment also increases stability parameters $R_{on}(t)$, $R_{off}(t)$. Annealing at temperatures above 350°C leads to a significant increase in resistive switching voltages. This process is determined by a significant increase in ρ of the NC during annealing in the temperature range from 400 to 500°C.

Keywords: Resistive switching, memristors, nanocomposite, lithium niobate.

DOI: 10.61011/PSS.2024.10.59623.199

1. Introduction

Structures having affects of resistive switching (RS) are rather attractive to make new generation of nonvolatile memory with large density and low power consumption during information writing/reading [1–3]. On other hand such structures can be used to create memristors, which functionally emulate action of synapse (combination) in biological neuron network (brain) [3–7]. In last years great attention for use as memristive devices was attracted to such structures as metal-dielectric-metal (M/D/M), this ensures use of memristor massives in matrix design as elements of multilevel memory when solving objective of artificial intellect: identification of images and natural language, decisions making, generalization, forecasting etc. [8–19].

To date, rather rich experimental material was accumulated, which contains, among other things, the evidence base for the key role of oxygen vacancies (ions) in the resistive switching of many objects based on metal oxides. It is interesting that in case of MOM structures RS is due to processes electrical migration of oxygen vacancies in dielectric interlayer, or metal cations (such as Cu, Ag) into dielectric from active electrode [4,5,19–22]. As a result filamentary conductive channels (filaments) are formed (destroyed) in the dielectric layer. Spatial position of filaments is accidental, and in many cases is determined by the defects in dielectric interlayer on interface M/D. This circumstance is one of the main causes of significant instability of properties of memristors during their cyclic RSs [2,14].

In case of structures metal-nanocomposite-metal (M/NC/M) the transition into conductive state in dielectric region of NC composition ($x < x_c$) is under determining effect of percolation chains set by spatial position and concentration of metal nanogranules, this in turn shall ensure higher stability of switchings. Such approach ensures in structures M/NC/M based on NC $(Co_{40}Fe_{40}B_{20})_x(LiNbO_3)_{100-x}$ to implement the bipolar resistive switching with ratio $R_{off}/R_{on} \approx 100$, where R_{off} — high-resistance, and R_{on} — low-resistance resistive state [23–25]. At that number of stable cycles of RS (endurance) exceeds 106, and holding time of resistive states — over 10^4 s [24,25]. Besides, synthesized M/NC/M-structures have high degree of plasticity of resistive states (possibility to induce multiple stable intermediate resistive states in range between R_{off} and R_{on}) [25–28]. Studies of structure M/NC/M using high-resolution TEM showed presence of dielectric interlayer a-$LiNbO_3$ 10−15 nm thick which is formed at initial stage of nanocomposite growth on bottom metal electrode as a result of self-organization process [29,30]. Therefore, more correctly the structure M/NC/M can be presented as M/NC/D/M, where as dielectric (D) the interlayer a-$LiNbO_3$ is used. Actually, structures M/NC/D/M, where a-$LiNbO_3$ 10−15 nm thick is formed by its sputtering from original target, demonstrate similar memristive properties.

Supposition on formation of multi-filament RS in structures M/NC/D/M due to conductive channels of NC provide high degree of variation in properties optimization due to use of NC with different composition of metallic and dielectric phases. NC $(Co_{40}Fe_{40}B_{20})_x(SiO_2)_{100-x}$ the most

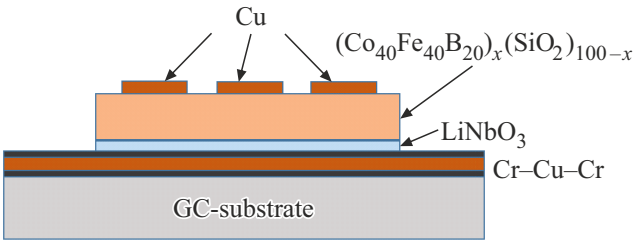

Figure 1. Topology of the experimental samples M/NC/D/M.

studied, from one hand it has homogeneous nanogranular structure [31], and on the other hand rather high thermal stability of structural and electrical properties [32]. Actually, the made studies identified that in structure $Cu/(Co_{40}Fe_{40}B_{20})_x(SiO_2)_{100-x}/LiNbO_3/Cr/Cu/Cr/glass$-ceramic in range of concentrations of metallic phase of NC from 18 to 43 at.% the reversible bipolar switching are observed. The voltage of switching from R_{off} to R_{on} state and vice versa reaches ± 4 V at $x = 37-42$ at.%. Ratio $R_{off}/R_{on} \approx 100$, endurance over 10^4 of reversible switching cycles. But, some relaxation of values of time dependences of induced resistive states is identified, this is associated with the electrical properties of functional interlayer $LiNbO_3$, which in initial state is complex heterogeneous structure, where heterogeneouss NbO_2 are embedded in the amorphous matrix [paper is in editorial board]. One of possible methods to change the memristive properties of complex, multi-component and nanofragmented structures is heat treatment.

So, main objective of this paper is identification of heat treatment effect on the memristive properties of structure $M/(CoFeB)_x(SiO_2)_{100-x}/LiNbO_3/M$.

2. Samples and study methods

By method of ion-beam sputtering the capacitance structures M/NC/D/M were obtained, where as NC films $(Co_{40}Fe_{40}B_{20})_x(SiO_2)_{100-x}$ were used (hereinafter these composites will be designated as $(CoFeB)_x(SiO_2)_{100-x}$) as D — $LiNbO_3$. As layers of metallic electrodes (M) the three-layer conductors Cr-Cu-Cr were used as bottom electrode, top electrode is formed from Cu film.

Three process operations of ion-beam sputtering were used to obtain the experimental samples. At first stage on glass-ceramic substrate multi-layer structure Cr-Cu-Cr was deposited. Prior to sputtering the ion cleaning of the substrate surface was performed, then the wafers were moved to Cr target sputtering position, where a chromium metal film ~ 100 nm thick was deposited for 10 min. Then, using a rotationally controlled substrate holder, the samples were moved to the zone of Cu deposition from the corresponding target, where copper film ~ 1000 nm thick was deposited for 30 min, followed by a repeat of the Cr layer deposition operation (~ 100 nm for 10 min).

At second stage the glass-ceramic substrates with deposited metal coating (4 wafers with size 60×48 mm^2) were arranged in row to obtain the deposition surface area 240×48 mm^2. The substrates were covered with a shadow screen with 8 mm diameter holes arranged in 24 rows of 6 holes per row. $LiNbO_3$ film was sputtered from original target. Deposition was performed with substrate holder turntable rotation with speed one turn for five minutes with substrates passage in sputtering zone of target $LiNbO_3$. Three deposition cycles were performed. Per one cycle the coating thickness reaches about 5 nm. The dielectric interlayer was synthesized in work gas atmosphere ($P_{Ar} \sim 3.9 \cdot 10^{-4}$ Torr) with oxygen addition $P_{O2} \sim 1.9 \cdot 10^{-5}$ Torr.

NC film was deposited from composite target where on wafer of alloy $Co_{40}Fe_{40}B_{20}$ with size $280 \times 80 \times 10$ mm^3 unevenly 13 rectangular wafers of single-crystal quartz with size $80 \times 10 \times 2$ mm^3 were arranged. Such composite target ensures smooth and continuous change of concentration of metallic phase of composite along surface of substrates [33,34]. During the synthesis of NC layer, oxygen at pressure $P_{O2} \sim 0.9 \cdot 10^{-5}$ Torr was added to the working gas atmosphere ($P_{Ar} \sim 3.9 \cdot 10^{-4}$ Torr). The film ~ 250 nm thick was formed during sputtering time of 15 min. The variation of metallic phase concentration in the composite was from 18.9 to 42.1 at.%.

Top contact pads made of Cu on multilayer structure were applied through a metal mask with hole size 0.5×0.2 mm^2 using the technology described above.

Note that the vacuum ion-beam sputtering unit has an oil-free pumping system. Preliminary vacuum is at least $1 \cdot 10^{-6}$ Torr. Particularly pure gases of at least 99.999% were used for sputtering. Prior to sputtering the target surface was pre-sputtered, and the substrates were ion cleaned.

The elemental composition of NC was determined using Oxford INCA Energy 250 energy-dispersive X-ray attachment on JEOL JSM-6380 LV scanning electron microscope. The accuracy of determining the composition of the samples was determined by their size, discrete location on the substrates and was $x \pm 1$ at.%. The structural analysis was performed by X-ray method on X-ray diffractometer BRUKER D2 PHASER.

The current-voltage characteristic (CVC) of M/NC/M structures and their memristive properties were measured using KEITHLEY 2450 multifunctional source-measuring device and an analytical probe station in current-limited mode. CVC of structures MNC/M were measured with grounded bottom electrode and bias voltage sweep U of top electrode as per linear law in sequence from $0 \rightarrow +U_{max} \rightarrow -U_{max} \rightarrow 0$ V with step 0.1 V. The rate of voltage change was 10 V/s.

The heat treatment was performed using the tungsten resistive heater in vacuum at residual gas pressure at least 10^{-5} Torr.

3. Results and discussion

As object of study the structure $Cu/(Co_{40}Fe_{40}B_{20})_{35.5}(SiO_2)_{64.5}/LiNbO_3/Cr/Cu/Cr/glass$-ceramic was selected having optimal memristive properties in initial state.

X-ray characterization of structure of nanocomposite $(CoFeB)_x(SiO_2)_{100-x}$ (NC) and dielectric $LiNbO_3$ (D) was performed on films with thickness about 1 μm deposited in surface of wafers of single-crystal Si (100).

X-ray diffraction did not reveal the crystalline structure of NC during heat treatment up to 500°C (Figure 2). Presence of small-angle X-ray diffraction from NC $(CoFeB)_{38.9}(SiO_2)_{61.1}$ films confirms a fairly uniform arrangement of metal granules in NC. As per position of maximum one can evaluate average distance between granules, i.e. actually width of dielectric layer between metal nanoparticles in NC. These evaluations provide values of about 3.4 nm in initial state and increase to 3.8 nm after annealing at 500°C (insert in Figure 2). Actually, at NC annealing temperature increasing on one hand extensive diffusion process of redistribution of embedded atoms of foreign phase on the interface of metal particles and dielectric matrix occurs, and from other hand we are rather close to temperature (500–550°C), at which crystallization of amorphous metal particles of alloy $Co_{40}Fe_{40}B_{20}$ in this NC is observed, this results in catastrophic changes in structure and formation of metal nanocrystals with size up to several tens of nanometers [23]. Which of the given processes determines the distance increasing between metal particles of NC, shall be further studied and does not affect the interpretation of this paper results.

X-ray diffraction from film $LiNbO_3$ (Figure 3) up to temperatures of heat treatment 450°C is most accurately described at its modeling by environment where nanocrystals of monoclinic Nb_2O_5 are embedded into the amorphous matrix. In process of crystallization during heat treatment at 500°C for 60 min the crystalline phase $LiNbO_3$ is formed. Note that the diffraction peak from nanoregions Nb_2O_5 decreases their intensity upon heat treatment temperature increasing to 350°C, and then up to temperature 450°C, intensity of this maximum does not change (insert in Figure 3). From these observations we can suppose nanoregions Nb_2O_5 destruct at rather moderate annealing temperatures (300–350°C), as a result degree of homogeneization of amorphous phase increases, it further at 500°C crystallizes into crystalline structure $LiNbO_3$.

Analysis of change in CVC of structure $Cu/(Co_{40}Fe_{40}B_{20})_{35.5}(SiO_2)_{64.5}/LiNbO_3/Cr/Cu/Cr/glass$-ceramic and its basic memristive properties depending on temeperature of heat treatment for 60 min, presented in Figures 4 and 5, ensures determination of some interesting features. It is identified that below annealing temperature 250°C change in parameters of bipolar resistive switching results in minor increase in switching voltages and decrease in values of relative change in induced resistances. At that basic features of CVC do not change. During heat treatment at temperatures 300°C and 350°C significant decrease in switching voltages occurs, values R_{off}/R_{on} increase, but no specific value on the CVC is found for the $U_{on\text{-}off}$ switching voltage. At annealing above 400°C the memristive effect in structure degrade.

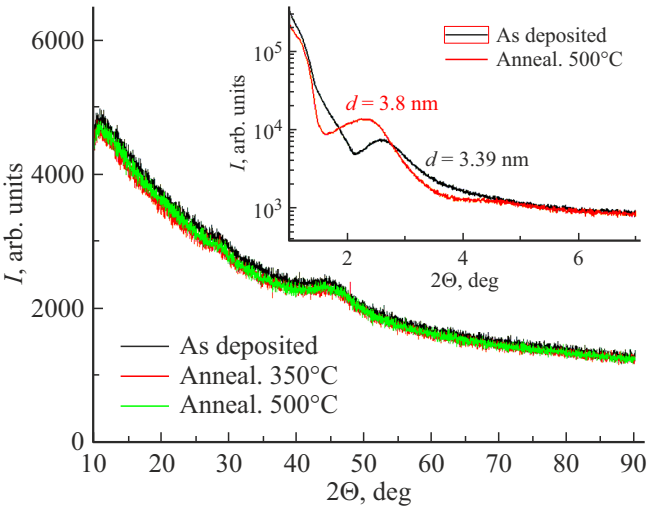

Figure 2. X-ray diffraction patterns of films NC $(CoFeB)_{38.9}(SiO_2)_{61.1}$ in initial state and after heat treatment for 60 min. Insert contains small-angle diffraction patterns of films NC $(CoFeB)_{38.9}(SiO_2)_{61.1}$ in initial state and after heat treatment for 60 min.

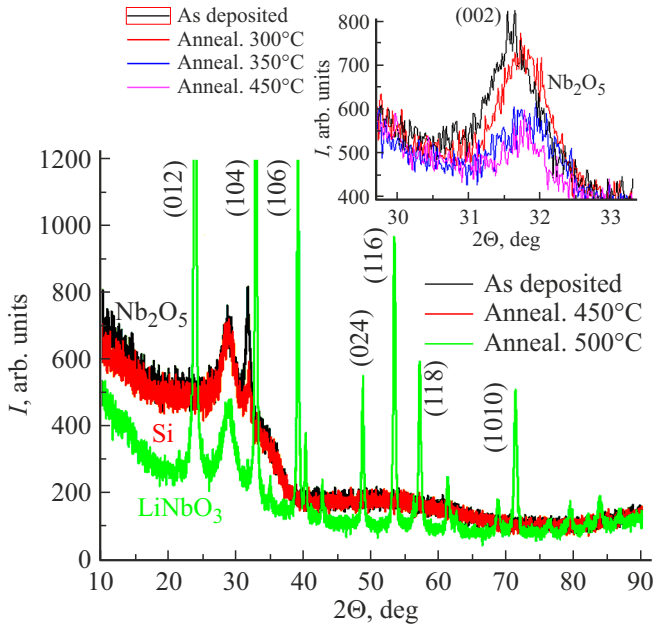

Figure 3. X-ray diffraction patterns of film $LiNbO_3$ in initial state and after heat treatment for 60 min. The insert presents the diffraction pattern from film $LiNbO_3$ in initial state and after heat treatment for 60 min in region of maximum corresponding to phase Nb_2O_5.

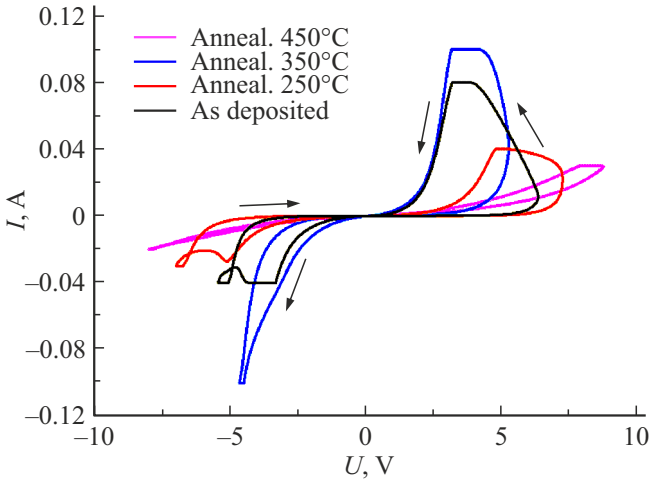

Figure 4. CVC of memristive element $Cu/(Co_{40}Fe_{40}B_{20})_{35.5}(SiO_2)_{64.5}/LiNbO_3/Cr/Cu/Cr/glass\text{-}ceramic$ in initial state and after heat treatment for 60 min.

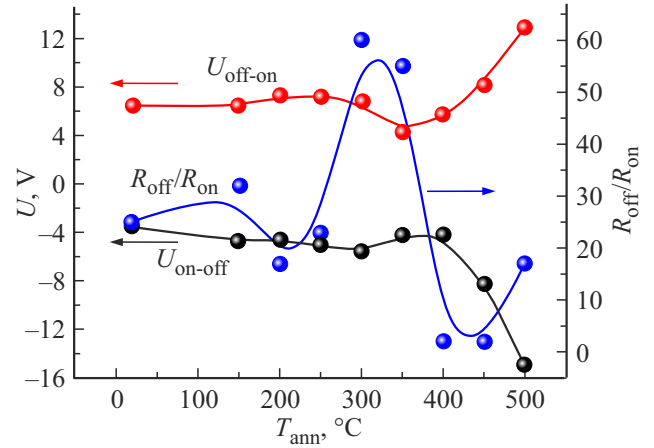

Figure 5. Concentration dependences of parameters R_{off}/R_{on}, $U_{off\text{-}on}$ and $U_{on\text{-}off}$ for structure $Cu/(Co_{40}Fe_{40}B_{20})_{35.5}(SiO_2)_{64.5}/LiNbO_3/Cr/Cu/Cr/glass\text{-}ceramic$ in initial state and after heat treatment for 60 min.

Basic identified disadvantage of studied structure in initial state was low time stability of states induced in it. Analysis of time dependences of induced resistive states of structure under study, presented in Figure 6, showed that with annealing temperature increasing the stability of this parameter increases.

To study issue of RS parameters change of studied memristive structure $Cu/(Co_{40}Fe_{40}B_{20})_{35.5}(SiO_2)_{64.5}/LiNbO_3/Cr/Cu/Cr/glass\text{-}ceramic$ the quasistatic CVC were measured. Voltage step was 0.1 V. At current voltage for 10 s 10 values of electrical resistance were measured (Figure 7). These values were treated by calculation of relative change in resistance at fixed voltage on sample (Figure 8).

Analysis of these dependences shows that in initial state at positive offset of voltage on top electrode the irreversible changes in resistive state (decrease in values R) are observed at rather insignificant voltages and continue with increasing rate to ~ 3.5 V. In this voltage range the dependence $(R_{i+1} - R_i)/R_i$ can be easily presented as superposition of two resonance curves. Transition from state R_{on} to R_{off} (negative voltage on top electrode) has some range of voltage of 0 to -2 V, where the irreversible changes in voltage are insignificant. And only at voltages from -2 to -4 V the structure transition from low-resistance into high-resistance state. This is in good correlation with time dependences of induced resistive states (Figure 6, dark curves), where for sample in initial state the rate of decreasing of $R_{off}(t)$ is higher then increasing of $R_{on}(t)$. After heat treatment of sample at 250°C for 60 min there is decrease in energy distribution of transition process $R_{off} \rightarrow R_{on}$ at positive voltage on top electrode,

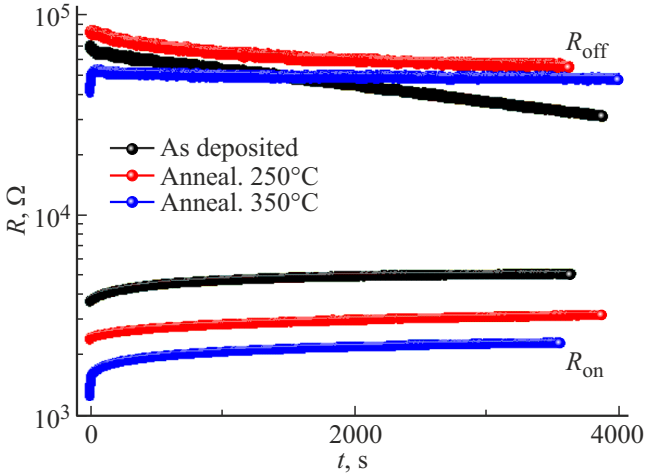

Figure 6. Time dependence of induced resistive states for structure $Cu/(Co_{40}Fe_{40}B_{20})_{35.5}(SiO_2)_{64.5}/LiNbO_3/Cr/Cu/Cr/glass\text{-}ceramic$ in initial state and after heat treatment for 60 min.

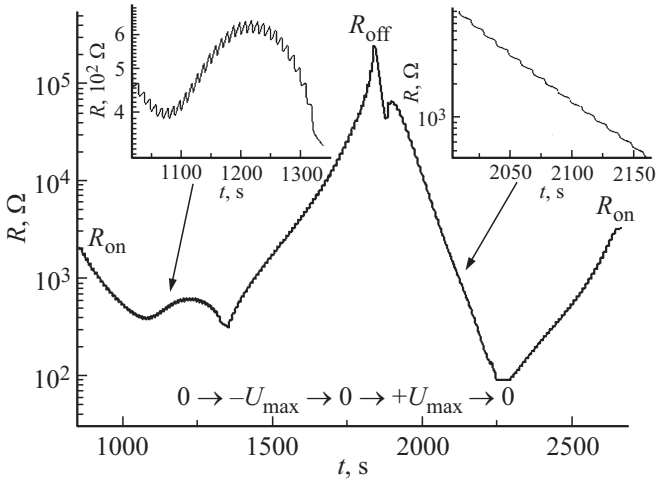

Figure 7. Time dependence of electric resistance change of structure $Cu/(Co_{40}Fe_{40}B_{20})_{35.5}(SiO_2)_{64.5}/LiNbO_3/Cr/Cu/Cr/glass\text{-}ceramic$ at change in applied voltage. The inserts present fragments of curves with zoom in to demonstrate nature of dependence in different sections.

and transition voltage moves in range of high voltages. This change is well correlated with relative change in CVC dependences (Figure 4) and increase in stability of induced states (Figure 6, red curves). Annealing temperature increasing to 350°C somewhat decreases the voltage of transitions $R_{on} \rightarrow R_{off}$ and $R_{off} \rightarrow R_{on}$ relative to samples annealed at 250°C, especially in region of high-resistance RS. In same region there are two maxima on dependence of relative rate of change in electrical resistance on voltage at −2.5 V and −3.5 V. But, these changes do not result in relaxation of resistive states of sample at low voltage of measurement of resistive state, and, as a result, the time stability of induced R stays high (Figure 6, blue curves).

Increase in stability of dependences $R_{on}(t)$ and $R_{off}(t)$ has positive effect on characteristics of plasticity of resistive states of structure under study (Figure 9). Besides that the possibility is kept to induce practically any resistive states R_i in range between values R_{on} and R_{off} after structure annealing up to 350°C, but dependences $R_i(t)$ become more stable.

Cyclic endurance of samples after heat treatment up to 300°C also has no significant changes and reaches at least 10^4 reversible cycles of RS (Figure 10).

Such various behaviour of the structure under study can not be explained based on the structural changes in D interlayer and NC, shown in Figures 2 and 3. Some improvement in the complex of set of memristive properties observed during annealing up to 350°C, is in well correlation with decrease in size and density of inclusions of monoclinic nanoparticles Nb_2O_5 in matrix a-$LiNbO_3$. But significant changes in structure neither in a-$LiNbO_3$, nor in NC $(Co_{40}Fe_{40}B_{20})_{35.5}(SiO_2)_{64.5}$ in temperature range 350–450°C were not revealed by X-ray diffraction studies. In this case it is interesting to observe change in electrical

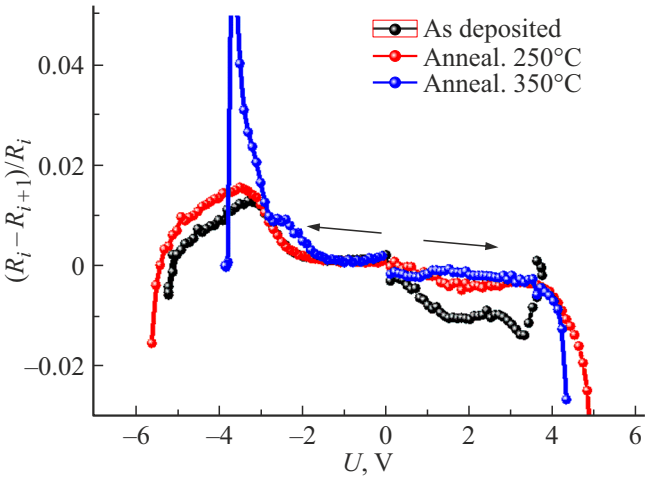

Figure 8. Relative rate of change in electrical resistance for structure Cu/$(Co_{40}Fe_{40}B_{20})_{35.5}(SiO_2)_{64.5}$/$LiNbO_3$/Cr/Cu/Cr/glass-ceramic depending of applied voltage in initial state and after heat treatment for 60 min.

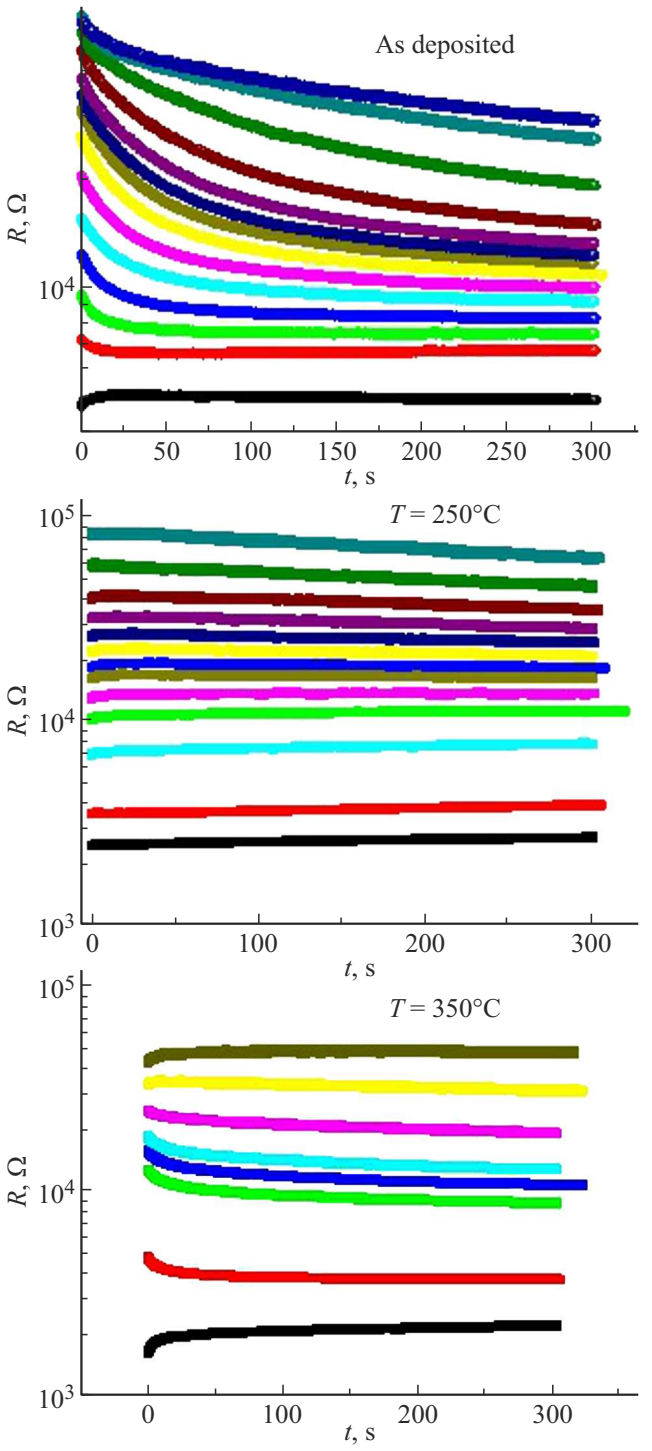

Figure 9. Time dependences of induced resistive states for memristive structures Cu/$(Co_{40}Fe_{40}B_{20})_{35.5}(SiO_2)_{64.5}$/$LiNbO_3$/Cr/Cu/Cr/glass-ceramic in initial state and after heat treatment for 60 min.

properties of NC after heat treatment (Figure 11). We see that after 400°C the specific resistance ρ of nanocomposite significantly (by several orders of magnitude) changes, at that its structure does not change. This can be explained by decrease in concentration of localized states in dielectric

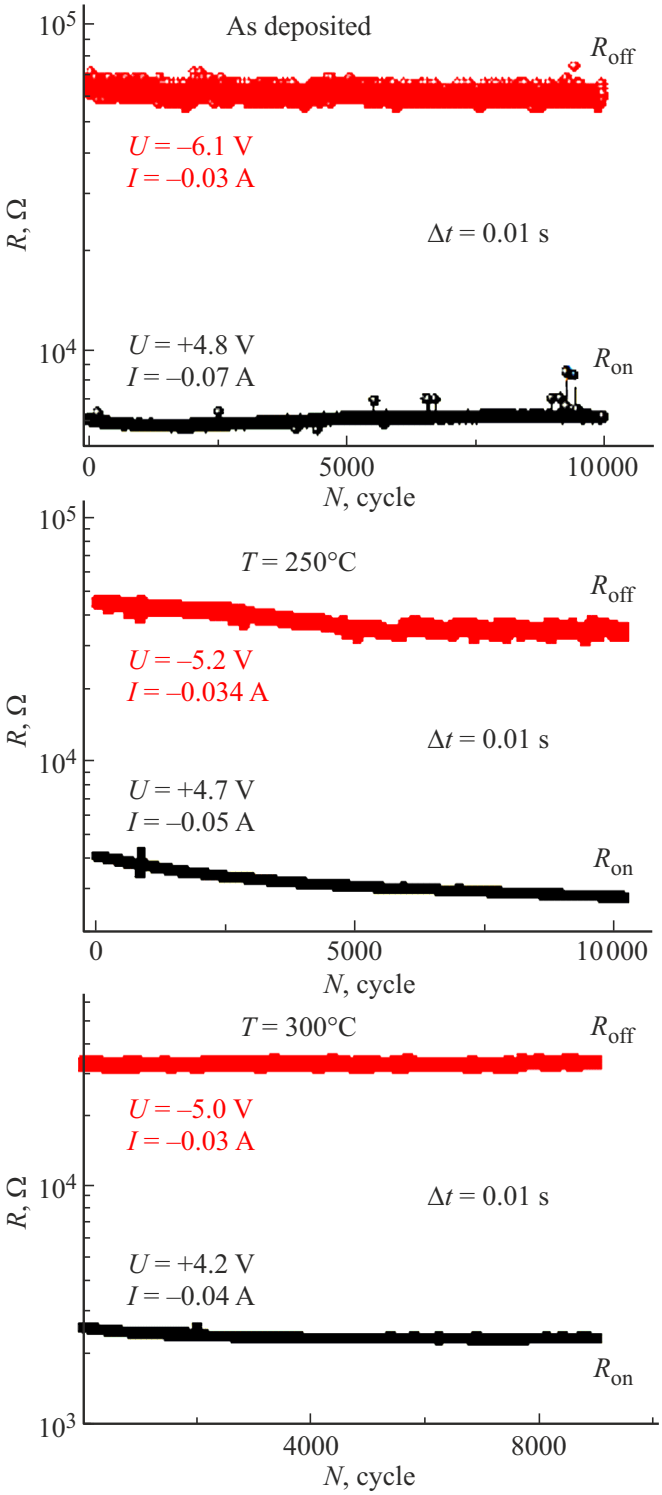

Figure 10. Switching of resistive states in memristive structures $Cu/(Co_{40}Fe_{40}B_{20})_{35.5}(SiO_2)_{64.5}/LiNbO_3/Cr/Cu/Cr/glass$-ceramic in initial state and after heat treatment for 60 min.

matrix of NC, participating in electrical transition [23]. It is clear that in that case voltage on interlayer a-$LiNbO_3$ decreases, and we register significant increase in RS voltage (measured on entire structure).

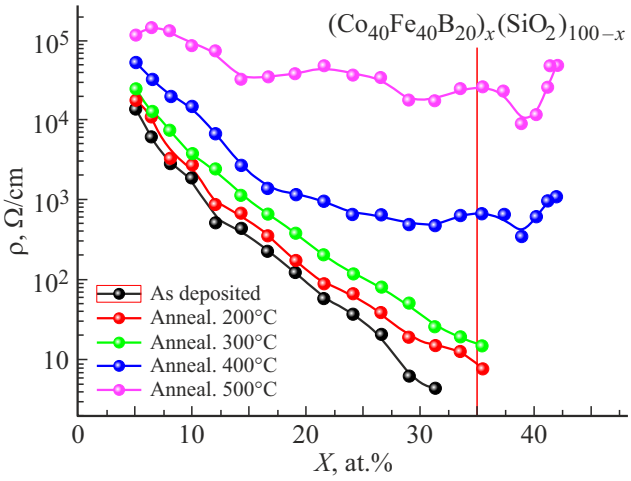

Figure 11. Concentration dependences of specific electrical resistance of NC $(Co_{40}Fe_{40}B_{20})_x(SiO_2)_{100-x}$ after heat treatment at different temperatures for 60 min.

4. Conclusion

Studies of heat treatment effect on memristive properties of structure $Cu/(Co_{40}Fe_{40}B_{20})_{35.5}(SiO_2)_{64.5}/LiNbO_3/Cr/Cu/Cr/glass$-ceramic showed that annealing up to 350°C does not affect the cyclic endurance of samples but increase ratio R_{off}/R_{on} and decrease values of RS voltages. In that case, heat treatment improves stability of parameters $R_{on}(t)$, $R_{off}(t)$ and time stability of induced resistances in range between values R_{on} and R_{off} during measurements of plasticity of structure resistive states. We suppose that this is associated with increase in degree of homogenization of amorphous phase of dielectric interlayer of lithium niobate due to decrease in size and concentration of nanoregions Nb_2O_5, disributed in amorphous matrix $LiNbO_3$ at annealing temperatures (300–350°C).

Heat treatment at temperatures above 350°C result in significant increase in RS voltages. This process is determined by significant (by several orders of magnitude) increase in specific resistance ρ of NC during annealing of 400 to 500°C. Such degradation of properties is associated with decrease in the concentration of localized states in the dielectric matrix of NC involved in the process of electrotransport as a result of thermal exposure.

Funding

This study was supported by the Ministry of Science and Higher Education of the Russian Federation under State Assignment FZGM-2023_0006.

Conflict of interest

The authors declare that they have no conflict of interest.

References

[1] J.S. Lee, S. Lee, T.W. Noh. Appl. Phys. Rev., **2**, 031303 (2015).
[2] D. Ielmini. Semicond. Sci. Technol., **31**, 063002 (2016).
[3] D. Ielmini, R. Waser. Resistive Switching: From Fundamentals of Nanoionic Redox Processes to Memristive Device Applications. Wiley-VCH Verlag Weinheim, Germany (2016). 755 p.
[4] J. del Valle, J.G. Ramirez, M.J. Rozenberg, I.K. Shuller. J. Appl. Phys., **124**, 211101 (2018).
[5] Y. Li, Z. Wang, R. Midya, Q. Xia, J.J. Yang. J. Phys. D: Appl. Phys., **51**, 503002 (2018).
[6] S.G. Kim, J.S. Han, H. Kim, S.Y. Kim, H.W. Jang. Adv. Mater. Technol., **3**, 1800457 (2018).
[7] S.H. Tan, P. Lin, H. Yeon, S. Choi, Y. Park, J. Kim. APL Materials **6**, 120901 (2018).
[8] C. Li, M. Hu, Y. Li, H. Jiang, N. Ge, E. Montgomery, J. Zhang, W. Song, N. Davila, C.E. Graves, Z. Li, J.P. Strachan, P. Lin, Z. Wang, M. Barnell, Q. Wu, R.S. Williams, J.J. Yang, Q. Xia. Nat. Electr., **1**, 52 (2018).
[9] Z. Wang, S. Joshi, S.E. Savel'ev, W. Song, R. Midya, Y. Li, M. Rao, P. Yan, S. Asapu, Y. Zhuo, H. Jiang, P. Lin, C. Li, J.H. Yoon, N. Upadhyay, J. Zhang, M. Hu, J.P. Strachan, M. Barnell, Q. Wu, H. Wu, S. Williams, Q. Xia, J.J. Yang. Nat. Electr., **1**, 137 (2018).
[10] C. Li, D. Belkin, Y. Li, P. Yan, M. Hu, N. Ge, H. Jiang, E. Montgomery, P. Lin, Z. Wang, W. Song, J.P. Strachan, M. Barnell, Q. Wu, R.S. Williams, J.J. Yang, Q. Xia. Nat. Commun., **9**, 2385 (2018).
[11] I. Boybat, M.L. Gallo, S.R. Nandakumar, T. Moraitis, T. Parnell, T. Tuma, B. Rajendran, Y. Leblebici, A. Sebastian, E. Eleftheriou. Nat. Commun., **9**, 2514 (2018).
[12] M.A. Zidan, Y.J. Jeong, J. Lee, B. Chen, S. Huang, M.J. Kushner, W.D. Lu. Nat. Electr., **1**, 411 (2018).
[13] M.A. Zidan, J.P. Strachan, W.D. Lu. Nat. Electr., **1**, 22 (2018).
[14] W. Banerjee, Q. Liu, H. Hwang. J. Appl. Phys., **127**, 051101 (2020).
[15] Y. Zhang, Z. Wang, J. Zhu, Y. Yang, M. Rao, W. Song, Y. Zhuo, X. Zhang, M. Cui, L. Shen, R. Huang, J. Yang. Appl. Phys. Rev., **7**, 011308 (2020).
[16] D. Ham, H. Park, S. Hwang, K. Kim. Nat Electron., **4**, 635 (2021).
[17] Q. Xia, J.J. Yang. Nat. Mater., **18**, 309 (2019).
[18] M. Zhuk, S. Zarubin, I. Karateev, Y. Matveyev, E. Gornev, G. Krasnikov, D. Negrov, A. Zenkevich. Front. Neurosci., **14**, 94 (2020).
[19] A. Mikhaylov, A. Belov, D. Korolev, I. Antonov, V. Kotomina, A. Kotina, E. Gryaznov, A. Sharapov, M. Koryazhkina, R. Kryukov, S. Zubkov, A. Sushkov, D. Pavlov, S. Tikhov, O. Morozov, D. Tetelbaum. Adv. Mater. Technol., **5**, 1900607 (2020).
[20] D.-H. Kwon, K.M. Kim, J.H. Jang, J.M. Jeon, M.H. Lee, G.H. Kim, X.-S. Li, G.-S. Park, B. Lee, S. Han, M. Kim, C.S. Hwang. Nat. Nanotechnol., **5**, 153 (2010).
[21] J.-Y. Chen, C.-W. Huang, C.-H. Chiu, Y.-T. Huang, W.-W. Wu. Adv. Mater., **27**, 5028 (2015).
[22] H. Jiang, L. Han, P. Lin, Z. Wang, M.H. Jang, Q. Wu, M. Barnell, J.J. Yang, H.L. Xin, Q. Xia. Sci. Rep., **6**, 28525 (2016).
[23] V.V. Rylkov, S. Nikolaev, V.A. Demin, A.V. Emelyanov, A.V. Sitnikov, K.E. Nikiruy, V.A. Levanov, M.Yu. Presnyakov, A.N. Taldenkov, A.L. Vasiliev, K.Yu. Chernoglazov, A. Vedeneev, Yu.E. Kalinin, A.B. Granovsky, V. Tugushev, A.S. Bugaev. J. Exp. Theor. Phys., **126**, 367 (2018).
[24] V.A. Levanov, A.V. Emel'yanov, V.A. Demin, K.E. Nikirui, A.V. Sitnikov, S.N. Nikolaev, A.S. Vedeneev, Yu.E. Kalinin, V.V. Rylkov. J. Commun. Technol. Electron., **63**, 496 (2018).
[25] K.E. Nikiruy, A.V. Emelyanov, V.A. Demin, A.V. Sitnikov, A.A. Minnekhanov, V.V. Rylkov, P.K. Kashakrov, M.V. Kovalchuk. AIP Advances, **9**, 065116 (2019).
[26] A.V. Emelyanov, K.E. Nikiruy, A.V. Serenko, A.V. Sitnikov, M.Yu. Presnyakov, R.B. Rybka, A.G. Sboev, V.V. Rylkov, P.K. Kashkarov, M.V. Kovalchuk. Nanotechnology, **31**, 045201 (2020).
[27] K.E. Nikiruy, I.A. Surazhevsky, V.A. Demin, A.V. Emelyanov. Phys. Status Solidi A, **217**, *18*, 1900938 (2020).
[28] I.A. Surazhevsky, V.A. Demin, A.I. Ilyasov, A.V. Emelyanov, K.E. Nikiruy, V.V. Rylkov, S.A. Shchanikov, I.A. Bordanov, S.A. Gerasimova, D.V. Guseinov, N.V. Malekhonova, D.A. Pavlov, A.I. Belov, A.N. Mikhaylov, V.B. Kazantsev, D. Valenti, B. Spagnolo, M.V. Kovalchuk. Chaos, Solitons and Fractals, **146**, 110890 (2021).
[29] V.V. Rylkov, S.N. Nikolaev, K.Y. Chernoglazov, V.A. Demin, M.Y. Presnyakov, A.L. Vasiliev, V.V. Tugushev, A.B. Granovsky, A.V. Sitnikov, Y.E. Kalinin, N.S. Perov, A.S. Vedeneev. Phys. Rev. B, **95**, *14*, 144202 (2017).
[30] A.V. Sitnikov, I.V. Babkina, Yu.E. Kalinin, A.E. Nikonov, M.N. Kopytin, A.R. Shakurov, O.I. Remizova, L.I. Yanchenko. ZhTF **92**, *9*, 1382 (2022). (in Russian).
[31] A.V. Sitnikov. Materialovedenie, **3**, 49 (2010). (in Russian).
[32] S.A. Gridnev, Yu.E. Kalinin, A.V. Sitnikov, O.V. Stogney. NELINEJNYE YAVLENIYA V NANO- I MIKROGETEROGENNYKH SISTEMAKH, OOO „Izdatel'stvo„ BINOM. Laboratoriya znanij", Moskva. (2012), p. 358. (in Russian).
[33] Yu.E. Kalinin, A.N. Remizov, A.V. Sitnikov. FTT, **46**, *11*, 2076 (2004). (in Russian).
[34] N. Domracheva, M. Caporali, E. Rentschler. Novel Magnetic Nanostructures: Unique Properties and Applications, Elsevier (2018), p. 490.

Translated by I.Mazurov